Direct Light Pattern Integration of Low-Temperature Solution-Processed All-Oxide Flexible Electronics

You Seung Rim,[†,∥] Huajun Chen,[†,∥] Yongsheng Liu,[†,‡] Sang-Hoon Bae,[†] Hyun Jae Kim,[§] and Yang Yang*[,†,‡]

[†]Department of Materials Science and Engineering and [‡]California NanoSystems Institute, University of California, Los Angeles, California 90095, United States and [§]School of Electrical and Electronic Engineering, Yonsei University, Seoul 120-749, Korea. [∥]These authors (Y.S.R. and H.C.) contributed equally to this work.

ABSTRACT The rise of solution-processed electronics, together with their processing methods and materials, provides unique opportunities to achieve low-cost and low-temperature roll-to-roll printing of non-Si-based devices. Here, we demonstrate a wafer-scale direct light-patterned, fully transparent, all-solution-processed, and layer-by-layer-integrated electronic device. The deep ultraviolet irradiation of specially designed metal oxide gel films can generate fine-patterned shapes of ~3 μm, which easily manifest their intrinsic properties at low-temperature annealing. This direct light patterning can be easily applied to the 4 in. wafer scale and diverse pattern shapes and provides feasibility for integrated circuit applications through the penetration of the deep ultraviolet range on the quartz mask. With this approach, we successfully fabricate all-oxide-based high-performance transparent thin-film transistors on flexible polymer substrates.

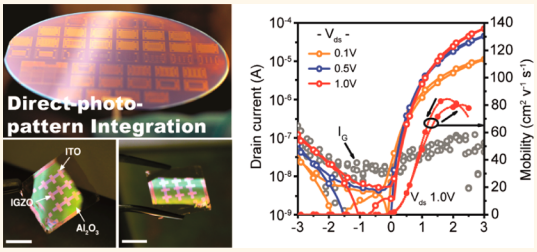

KEYWORDS: transparent electronics · solution process · thin-film transistor · patterning process · metal oxide semiconductor

Solution processing of inorganic electronic devices, including inkjet, screen printing, spray coating, and spin coating,[1−3] has been recognized as a potential substitute for traditional vacuum methods due to the low cost of nonvacuum facilities. Recently, solution-processed amorphous metal oxide semiconductors (AOSs) have attracted attention because of their unique structure and properties, including optical transparency, high electron mobility, flexibility, and good air stability.[4,5]

Despite these advantages, the low electrical performance and high-temperature processing (>500 °C) of solution-processed AOS devices are the biggest obstacles to their success,[5−9] as high-temperature processing is not suitable for flexible, conformal, smart skin, and roll-up electronics.[10,11] Although inkjet printing of AOSs has received attention for low-cost selective deposition, it still faces several problems, such as controllability of the shape, size, uniformity, and thickness of the deposited films. To overcome this obstacle on solution-processed AOSs, a photoinduced selective patterning technique of oxide films was reported to function in the oxide formation.[12,13] These works explored the approach of the photoreaction under the UVA range (mainly 365 nm) to form the cross-linking of a metal chelate for the selectivity in the leaching solvent. This process could only give an opportunity of patterning in the metal oxide solutions due to the low-energy support of the UVA region. One approach explained that low-temperature processing was possible. However, this effect was explained by the combustible reaction between fuels and oxidizers.[12] Regardless, the study of various oxide groups has not been done for all-oxide-based devices *via* multistep integration with ideal pattern mask systems.

Here, we report a direct light pattern (DLP) integration of functional metal oxide films including conductors, semiconductors, and insulators to achieve large-scale circuit integration through deep ultraviolet (DUV) processing. Our DUV system contains UVC ranges (184.9 nm (10%) and 253.7 nm (90%)) that produce higher energy to contribute to photoreactions compared to UVA processing. Energy absorbed by our specially designed chemical structures could

* Address correspondence to yangy@ucla.edu.

Received for review August 7, 2014 and accepted September 8, 2014.

Published online September 08, 2014
10.1021/nn504420r

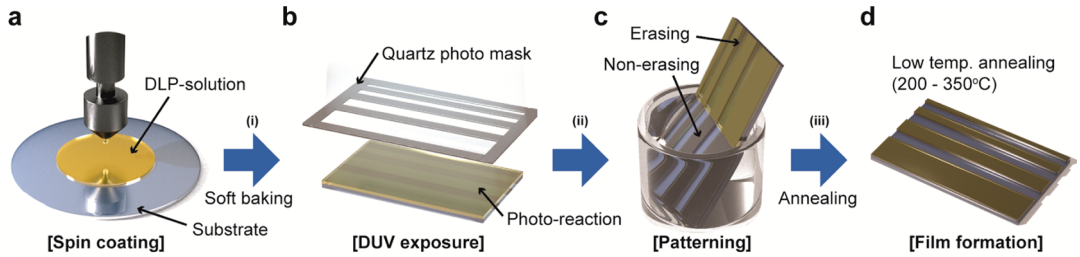

Figure 1. Schematic of direct light patterning and film formation using chemically modified metal salt precursors. (a) DLP-IGZO, Al_2O_3, and ITO solutions are spin-coated on desired substrates. (b) Exposure of soft-baked (100 °C) samples with a quartz mask under DUV. (c) Dipping samples in methanol/acetic acid, leaving only DUV-exposed regions. (d) Patterned films are annealed at desired temperatures.

promote metal oxide formation[6] and patterning simultaneously. The proposed technique (Figure 1) can dramatically reduce the processing steps of device integration and avoid toxic and high-cost chemicals, such as photoresists, developers, removers, and etchants, as would be used in traditional photolithography. Additionally, delicately designed metal oxide precursors exhibit strong exothermic reaction-based low-temperature formation by the combustion process between our additive and metal nitrate precursors.[7,14] Interestingly, this reaction could be initiated by DUV irradiation so that high-quality metal oxide could be achieved at low temperature. For these abilities, we successfully proved the origin of simultaneous photopatterning and low-temperature formation of insulators, semiconductors, and conductor materials, with which we demonstrated all-oxide-based transparent transistors. With the optimized DLP process, indium−gallium−zinc oxide (DLP-IGZO) thin-film transistors (TFTs) with a high mobility greater than 15 $cm^2 V^{-1} s^{-1}$ were achieved. Additionally, DLP-based tin-doped indium oxide (ITO) and aluminum oxide (Al_2O_3) as transparent conductor and insulator films had excellent electrical properties, confirming the universality of the DLP process in metal oxide systems. Based on the integration of ITO (electrodes), Al_2O_3 (dielectric), and IGZO (semiconductor), we demonstrated the first TFT formed entirely from a DLP process with a high mobility of 84.4 $cm^2 V^{-1} s^{-1}$ at a low driving voltage (1.0 V).

RESULTS AND DISCUSSION

Typically, IGZO precursor solution is made by dissolving metal salts in organic solvents with a stabilizer to prevent the hydrolysis.[15,16] In contrast, our precursor has two additives, acetylacetone (AcAc) and ammonium hydroxide (NH_4OH), which allow for the formation of unique complexes and give strong absorption in DUV regions. To confirm the absorption enhancement and formation of DLP solutions, optical analysis was conducted, and UV−vis absorption spectra of the DLP-IGZO solution and the IGZO solution without additives are shown in Figure 2c. DLP-IGZO solution exhibited much broader absorption in the UV region from 200 to 400 nm than that of no-additive IGZO solution due to a $\pi-\pi^*$ transition in the chelate ring of AcAc.[17] This change in absorption illustrates that the chelate reaction has occurred between metal nitrates and AcAc, as presented in Figure 2a. Assisted by NH_4OH, metal ions occupy the position of the hydrogen atoms in the structural formula of AcAc to form the metal complex and the byproduct NH_4NO_3.

DUV irradiation led to a film solubility change in acetic acid/methanol solution: the gel film with good solubility becomes insoluble after DUV irradiation, indicating that a DUV irradiation-induced chemical reaction occurred. It is noteworthy that generated ozone (O_3) has only a slight role in the DLP process as the hard contact of the quartz pattering mask close to the gel film during irradiation. Also, DUV irradiation was performed in a nitrogen-filled glovebox (<0.1 ppm of O_2 and H_2O) for the DLP process, and samples formed the patterns regardless of the ambient gas (Figure S11). That is, the formation of the pattern shapes could be related to light-induced decomposition of the metal complex and the partial formation of a polymer.

To understand the chemical reaction that occurred during DUV irradiation, we performed Fourier transform infrared spectroscopy (FT-IR) analysis. As shown in Figure 2b, intense peaks assignable to AcAc were clearly visible: the peaks at 1766 and 1351 cm^{-1} were related to C═O stretching and CH_3 (C═O) in-phase bending, respectively.[18] After DUV irradiation, the peaks related to carbonyl groups diminished strongly. It could be attributed to the presence of photolysis in our complex owing to hydroxyl radical formation.[19,20] Hydroxyl radicals attack the unsaturated bond and cause the decomposition of the chelate structure.[21] Furthermore, the peaks representing NO_3^- (833 and 2393 cm^{-1}) and NH_4^+ (3166 cm^{-1}) also disappeared under DUV irradiation. The role of NH_4OH is two-fold in the precursor: First, it assists the chelate formation. Second, the byproduct of chelate formation, NH_4NO_3, acts as an oxidizer in combustion.[22] With AcAc as fuel to consume all of the available oxygen from NH_4NO_3, the redox reaction generates significant heat,[22] which

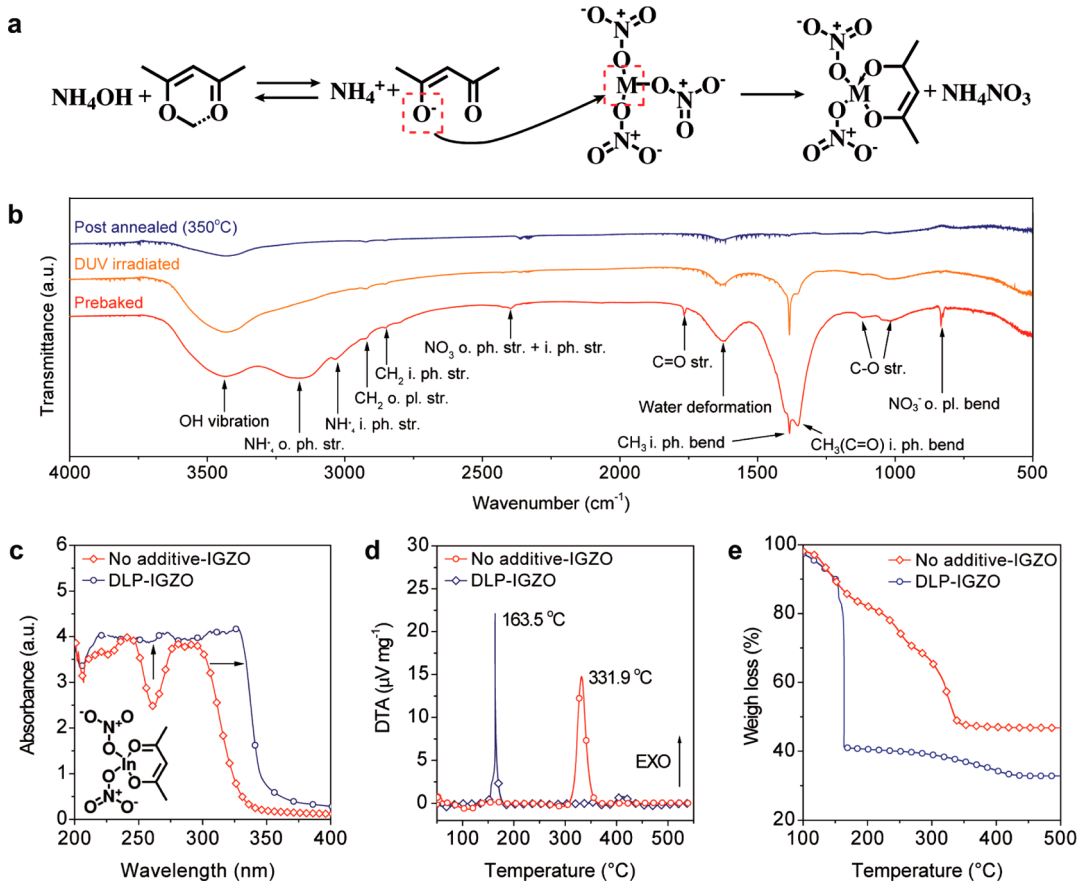

Figure 2. Precursor synthesis and photochemical and combustion reactions for the DLP process of IGZO thin films. (a) Chemical structure of a photoreactive metal organic precursor synthesized *via* complexation (M = In, Ga). The reaction for Zn is shown in Supporting Information Figure S1. (b) FT-IR spectra of prebaked at 100 °C (red), DUV irradiated (after prebaked, yellow), and postannealed (blue) DLP-IGZO films. (c) UV−vis absorption spectra, (d) TGA, and (e) DTA of no-additive and DLP-IGZO precursors.

assists with the elimination of organic residues and the formation of a metal oxide framework. It was supported by FT-IR results that C−H bonding (2921, 2853, and 1383 cm^{-1}) and C−O bonding (1113 and 1118 cm^{-1})[18] were reduced slightly after UV irradiation and fully disappeared after the final annealing.

It is fascinating to find that, in our system, combustion can be initiated by DUV, instead of conventional heat, as the temperature of the substrate during DUV irradiation is only around 70 °C (confirmed by the thermal couple attached to the substrate). To confirm the strong heat generation related to the combustion reaction, we used thermogravimetric and differential thermal analyses (TG-DTA) of DLP and no-additive IGZO precursors. The DLP precursor exhibits significantly lower decomposition temperature ($T \sim 163.5$ °C) than the no-additive precursor ($T \sim 331.9$ °C), as shown in Figure 2d,e. Unlike no-additive precursor, showing a broad peak for the oxide lattice formation,[7] the DLP-IGZO precursor exhibited a strong exothermic peak, corresponding to abrupt weight loss, indicating an efficient decomposition and transition to the oxide film. That is, our additive greatly reduced the annealing temperature to form a metal oxide film.

Therefore, DUV processing not only achieved photopatterning in IGZO gel films but also realized combustible reactions *via* external energy supply. The FT-IR spectrum of the prebaked film showed broad bands centered at 3443 and 1640 cm^{-1}, ascribed to basic hydroxyl groups and adsorbed molecular water. These peaks are slightly reduced after DUV irradiation and almost disappeared after postannealing due to dehydroxylation.

During DUV irradiation, the nonirradiated region still keeps its chelate structure and could be washed away easily using methanol/acetic acid solution due to salification between the hydrogen ion and chelate. This change in solubility of the precursor film can be applied to the direct light patterning process.

On the basis of this process, we successfully demonstrated a wafer-scale patterning process using additive oxide precursors, and multistep integration was also attainable, as shown in Figures 3a and 5. As shown *via* AFM (Figure 3b), the patterned region showed fine structures in exposed regions and clean removal of nonirradiated regions. We have also successfully demonstrated pattering shapes with a minimum feature size of 3 μm (Figures 3c and S10). Accordingly, the DLP

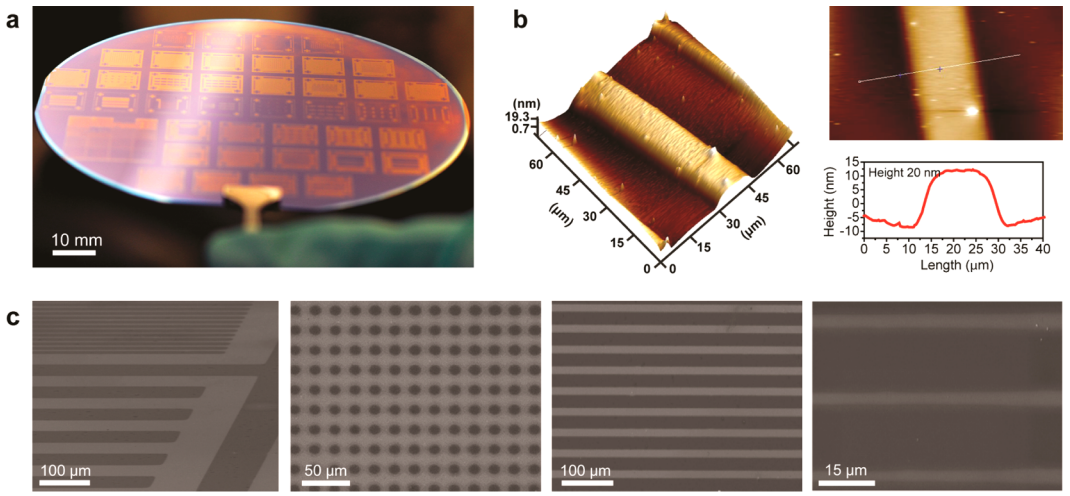

Figure 3. Demonstration of patterned DLP-IGZO films and large-scale circuit integration. (a) Image of wafer-scale full integration for transparent oxide electronics. (b) AFM images and cross-sectional profile of patterned DLP-IGZO film with a height of ~20 nm and a width of ~20 μm. (c) SEM images of various pattern shapes with negative and positive mask patterns. Dark regions indicate the SiO_2 surface, and light regions indicate patterned DLP-IGZO films. We successfully demonstrated the fine line width of 3 μm (bottom right side).

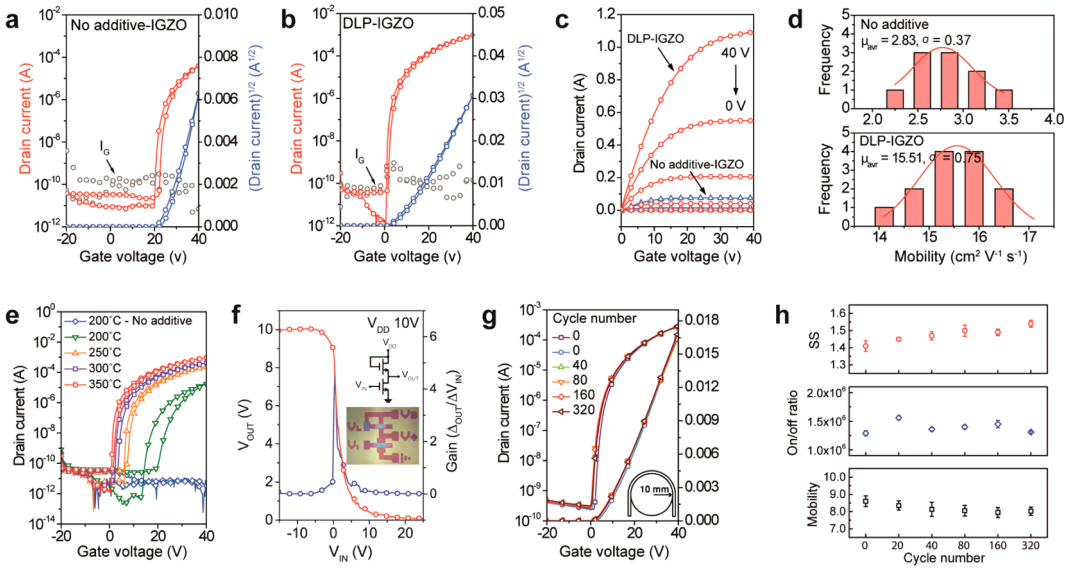

Figure 4. Electrical device performance of the DLP-IGZO semiconductor-based TFTs, circuit integration, and bending performance on a flexible array. (a–c) Transfer and output characteristics of no-additive IGZO and DLP-IGZO TFTs. (d) Histogram of the mobility for no-additive and DLP-IGZO TFTs processed at 350 °C. (e) Annealing temperature dependency of DLP-IGZO TFTs at 200–350 °C. (f) Enhancement mode inverter demonstration of the DLP-IGZO channel and DLP-ITO electrode combination (inset optical microscope image of DLP inverter). (g,h) Bending test of DLP-IGZO TFTs annealed at 300 °C on polyimide (20 × 20 mm) with a maximum bending radius of 10 mm.

process has high potential for an integrated circuit (IC) process, which can also form simple gratings of functional oxide films and various shape formation.

Optimized DLP-IGZO TFTs with 0.1 M AcAc and 0.2 M NH_4OH (Figures S2–S7) had much higher mobility of 15.51 ± 0.75 $cm^2 V^{-1} s^{-1}$ than no-additive IGZO TFT (2.83 ± 0.37 $cm^2 V^{-1} s^{-1}$), as shown in Figure 4. Turn-on voltage and on/off ratio of DLP-IGZO TFTs were 0 V and ~10^8, respectively, and the properties of SS and the hysteresis of the DLP-IGZO TFT were dramatically improved. Gate leakage current was found to depend on the existence of gate patterning or channel patterning,[12] in that a DLP-IGZO TFT achieved a low gate leakage current 10^6 orders of magnitude less than that of an unpatterned IGZO TFT (Figure S8). These results indicate that the DLP enables fine and clear patterns without the degradation of the films during the patterning process.

DLP-IGZO TFTs were evaluated for different annealing temperatures. Typically, solution-processed AOS TFTs show very low performance[5] even for high-temperature (>400 °C) annealing. Surprisingly, DLP-IGZO TFTs annealed at 200 °C still have a high saturation mobility of about 1.0 $cm^2 V^{-1} s^{-1}$ while IGZO TFTs with

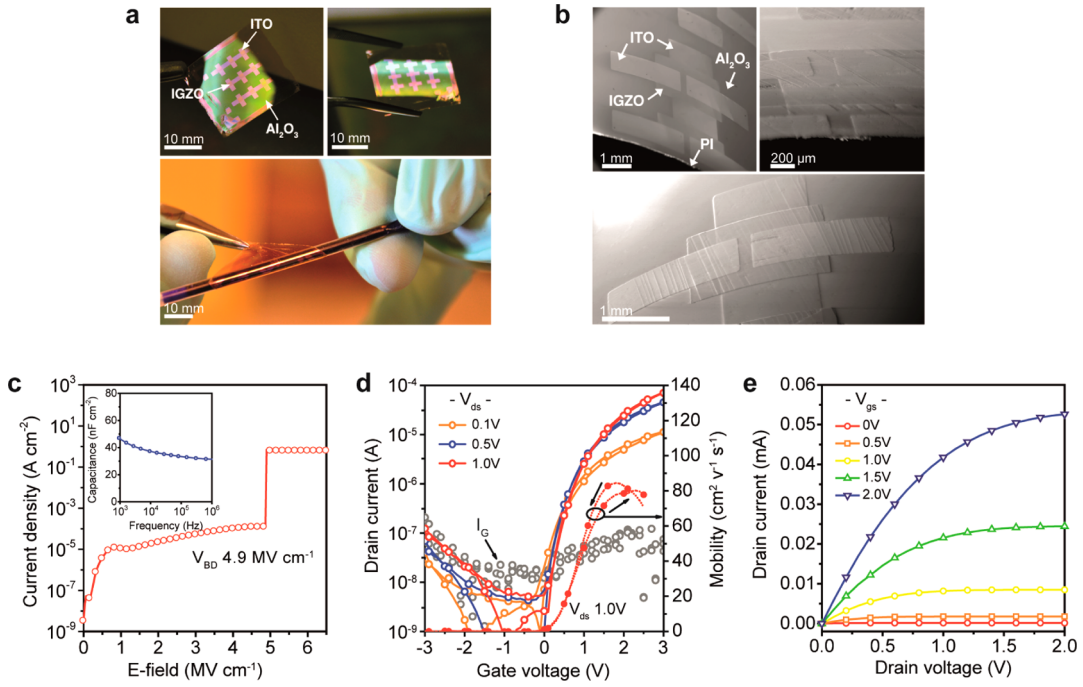

Figure 5. Transparent all-solution-processed IGZO TFTs using DLP multistep processing. (a) Photographs of integrated IGZO TFT with *S/D* and gate electrodes of ITO and the gate dielectric of Al_2O_3 on the PI substrate. (b) SEM images of bent IGZO TFTs on the PI substrate. (c) Current−voltage (*I*−*V*) and capacitance−frequency (*C*−*F*) measurement of Al/Al_2O_3/p++ Si-based MIM structure. (d) Transfer curves and mobility extraction of IGZO TFTs at V_{DS} of 0.1, 0.5, and 1.0 V on the PI substrate (*L* = 200 μm, *W* = 1000 μm). (e) Output characteristics of IGZO TFTs, showing clear pinch-off and current modulation with an increase of gate voltage.

no additive are inactive, as shown in Figures 4g and S6. As annealing temperature is increased from 200 to 350 °C, the mobility of TFTs increased from 1.0 to 16 $cm^2\ V^{-1}\ s^{-1}$ (Supporting Information Table S1). These are among the highest mobility values reported to date for air-stable conventional metal−salt complex precursor systems at low-temperature processing.

The formation of DLP oxide films could be applied not only to oxide semiconductors but also to transparent conductive oxide and dielectric materials. We have successfully demonstrated the enhancement mode inverter circuit with the alignment of DLP-ITO electrodes and the DLP-IGZO semiconductor layer (Figure 4f). The enhancement mode inverter showed good electrical modulation. On the basis of our results for different annealing temperatures, we fabricated DLP-IGZO TFTs on a polyimide substrate to confirm flexible application. The bending cycle properties are essential to evaluate the device stability on a repetitive flexion. The SS and mobility changed slightly over 320 cycles (Figure 4h) with a bending radius of 10 mm, confirming reasonable performance for flexible operation (S3).

To confirm DLP oxide-based TFTs, we demonstrated all-oxide-based transparent TFTs on a flexible substrate (Figure 5a). The DLP-Al_2O_3 dielectric showed a high breakdown voltage of ~4.9 MV cm^{-1} and good capacitance of 46.3 nF at 1 kHz (Figure 5c), and DLP-ITO has a resistivity of around $1.2 \times 10^{-2}\ \Omega\cdot$cm. X-ray diffraction (XRD) peaks in Figure S9 show amorphous structures for Al_2O_3, ITO, and IGZO thin films. Based on the structure (Figure 5b) of ITO (50 nm)/IGZO (20 nm)/Al_2O_3 (150 nm)/ITO (50 nm)/PI (18 μm), all DLP oxide-based TFTs had high mobility and high on/off ratio of ~84.4 $cm^2\ V^{-1}\ s^{-1}$ and greater than 10^5 at V_{DS} of 1.0 V and showed clear pinch-off behavior (Figure 5d,e). The high conduction band offset of the Al_2O_3 dielectric affects the reduction of the resistance of metal contacts and the channel layer. This effect could increase the mobility of the Al_2O_3 dielectric-based IGZO TFTs.[23]

CONCLUSION

In summary, we demonstrated the first fully oxide-based DLP-IGZO TFTs and wafer-scale circuit integration at low temperature. DUV processing not only supported the direct photopatterns on oxide gel films but also manifested a strong volatile reaction for low-temperature oxide formation. Furthermore, we demonstrated the formation of high-quality oxide films at low temperatures with fine patterning, yielding a minimum feature size of ~3 μm. Our DLP process could apply to a wide range of metal oxide systems (semiconductors, insulators, and conductors), showing good performance despite varying chemical structures and electrical properties. To support the applicability of this process to our large-scale integrated circuits, we demonstrated DLP-IGZO-based TFTs and multistep direct light processing for metal oxides. Fully DLP-based TFTs showed optical transparency and high

electrical performance at low driving voltage. Thus, we expect that the DLP process can overcome the main obstacles of solution-processed metal oxide electronics in terms of high-temperature film formation, significantly reduced cost, and free shape control. Furthermore, the DLP-based patterning process holds promise for controlling dimensions below the few micrometer scale and is ideal for circuit integration.

METHODS

Solution Synthesis of DLP Inorganic Oxide Solution. The 0.1 M DLP-IGZO solution was synthesized by dissolving 225.6 mg of indium nitrate hydrate ($In(NO_3)_3 \cdot xH_2O$, Aldrich, 99.999%), 21.3 mg of gallium nitrate hydrate ($Ga(NO_3)_3 \cdot xH_2O$, Aldrich, 99.999%), and 31.5 mg of zinc nitrate hydrate ($Zn(NO_3)_2 \cdot xH_2O$, Aldrich, 99.999%) in 10 mL of 2-methoxyethanol (2ME, Aldrich, 99%). Then, 20−200 μL of acetylacetone (aq) (AcAc, Aldrich, 99%) and 7−70 μL of ammonium hydroxide (aq) (NH_4OH, 28.0% NH_3 in water, Aldrich, 99.99%) were added in IGZO solutions. The total mole ratio was 9:1:2 of In, Ga, and Zn. After being stirred vigorously for 24 h at room temperature, the solutions appeared as light yellow transparent and homogeneous. All solutions were filtered through a 0.2 μm PTFE syringe filter (GE, Trevose, PA, USA). Detail methods for Al_2O_3 and ITO solution are shown in Supporting Information section S1.

Direct Light Patterning Technique. The DLP-IGZO, Al_2O_3, and ITO solutions were spin-coated on the substrate at 3000 rpm for 30 s. Spin-coated substrates were prebaked at 100 °C for 1 min, and then samples were exposed to DUV (184.9 nm (10%) and 253.7 nm (90%)) irradiation through a quartz mask for 10 min in air. After the samples were exposed to DUV, they were placed in a 20 mL methanol (CH_4O) + 1 mL acetic acid (CH_3COOH) solution for 5 s at room temperature and cleaned by DI water.

Fabrication of Devices. The substrates were cleaned in acetone and isopropyl alcohol sequentially. No-additive and DLP-IGZO solutions were spin-coated on SiO_2 (1000 Å)/boron-doped (p^{++})-doped Si wafers at 3000 rpm for 30 s and patterned *via* the direct light patterning process. We applied the same conditions for no-additive IGZO films as we did for the DLP-IGZO film, including prebaking and DUV exposure. To keep the same conditions of prebaked and DUV exposure, we applied the same procedures listed above to the no-additive IGZO film and patterned the film with the commercial photolithography process. The samples were then annealed at the desired temperatures (200−350 °C) for 3 h. The aluminum source and drain (*S*/*D*) electrodes (thickness = 100 nm) were deposited by thermal evaporation. The channel region was defined with a width (*W*) of 1000 μm and a length (*L*) of 200 μm. Detailed methods of all-solution-processed DLP-IGZO TFTs on polyimide (PI) substrate with an Al_2O_3 gate dielectric and ITO electrodes are shown in Supporting Information section S2.

Film and Device Characterization. The microstructures and morphologies of the films were investigated using digital optical microscopy (VHX-1000), atomic force microscopy (DIMENSION 5000 SPM, VEECO), X-ray diffractometer (Panalytical), and scanning electron microscopy (Nova 230, FEI). To examine different chemical compositions of DLP-IGZO films, we performed X-ray photoelectron spectroscopy (AXIS Ultra DLD, Kratos Analytical). To explore the chemical reaction in DLP-IGZO films, we measured transmission by Fourier transform infrared spectroscopy (420 FT-IR spectrophotometer, Jasco). The optical transmittance of the films was determined using a UV−visible spectrophotometer (Cary 50, Varian). Thermogravimetric analysis and differential thermal analysis of the solutions were performed using dried solutions at 50 °C in a vacuum oven using a TG-DTA analyzer (SDT Q600, TA Instruments). The electrical characteristics of the devices were measured in a dark box in ambient air using an Agilent 4155C semiconductor parameter analyzer. TFT measurements were performed by inducing a gate voltage (V_{GS}) of −20 to 40 V and a drain voltage (V_{DS}) of 30 V.

Conflict of Interest: The authors declare no competing financial interest.

Acknowledgment. This work was financially supported by a grant from the National Science Foundation (Grant No. ECCS-1202231, Program Director Dr. Paul Werbos, ECCS is a program under Engineering Division) and UCLA internal funds. The authors acknowledge the use of instruments at the Nano and Pico Characterization Lab at the California NanoSystems Institute, Molecular and Nano Archaeology (MNA) Lab and Molecular Instrumentation Center at UCLA. The authors sincerely thank Miss Renee M. Green for her help on the English editing, Dr. Chengyang Jiang for valuable discussions on the photochemical reaction, and Mr. Zehao Xue for drawing the schematic diagram.

Supporting Information Available: Synthesis and processing of Al_2O_3 and ITO, fabrication method of flexible devices, strain calculation of IGZO film, surface roughness of IGZO films, device parameters of IGZO TFTs with different conditions, TG-DTA, XPS, and XRD data of metal oxide solutions and films, optical images of patterned DLP-IGZO films. This material is available free of charge *via* the Internet at http://pubs.acs.org.

REFERENCES AND NOTES

1. Arias, A. C.; MacKenzie, J. D.; McCulloch, I.; Rivnay, J.; Salleo, A. Materials and Applications for Large Area Electronics: Solution-Based Approaches. *Chem. Rev.* **2010**, *110*, 3–24.
2. Pasquarelli, R. M.; Ginley, D. S.; O'Hayre, R. Solution Processing of Transparent Conductors: From Flask to Film. *Chem. Soc. Rev.* **2011**, *40*, 5406–5441.
3. Faber, H.; Butz, B.; Dieker, C.; Spiecker, E.; Halik, M. Fully Patterned Low-Voltage Transparent Metal Oxide Transistors Deposited Solely by Chemical Spray Pyrolysis. *Adv. Funct. Mater.* **2013**, *23*, 2828–2834.
4. Nomura, K.; Ohta, H.; Takagi, A.; Kamiya, T.; Hirano, M.; Hosono, H. Room-Temperature Fabrication of Transparent Flexible Thin-Film Transistors Using Amorphous Oxide Semiconductors. *Nature* **2004**, *432*, 488–492.
5. Fortunato, E.; Barquinha, P.; Martins, R. Oxide Semiconductor Thin-Film Transistors: A Review of Recent Advances. *Adv. Mater.* **2012**, *24*, 2945–2986.
6. Kim, Y.-H.; Heo, J.-S.; Kim, T.-H.; Park, S.; Yoon, M.-H.; Kim, J.; Oh, M. S.; Yi, G.-R.; Noh, Y.-Y.; Park, S. K. Flexible Metal-Oxide Devices Made by Room-Temperature Photochemical Activation of Sol−Gel Films. *Nature* **2012**, *489*, 128–132.
7. Kim, M.-G.; Kanatzidis, M. G.; Facchetti, A.; Marks, T. J. Low-Temperature Fabrication of High-Performance Metal Oxide Thin-Film Electronics *via* Combustion Processing. *Nat. Mater.* **2011**, *10*, 382–388.
8. Han, S.-Y.; Herman, G. S.; Chang, C.-h. Low-Temperature, High-Performance, Solution-Processed Indium Oxide Thin-Film Transistors. *J. Am. Chem. Soc.* **2011**, *133*, 5166–5169.
9. Rim, Y. S.; Jeong, W. H.; Kim, D. L.; Lim, H. S.; Kim, K. M.; Kim, H. J. Simultaneous Modification of Pyrolysis and Densification for Low-Temperature Solution-Processed Flexible Oxide Thin-Film Transistors. *J. Mater. Chem.* **2012**, *22*, 12491–12497.
10. Wang, C.; Hwang, D.; Yu, Z.; Takei, K.; Park, J.; Chen, T.; Ma, B.; Javey, A. User-Interactive Electronic Skin for Instantaneous Pressure Visualization. *Nat. Mater.* **2013**, *12*, 899–904.
11. Sekitani, T.; Someya, T. Stretchable, Large-Area Organic Electronics. *Adv. Mater.* **2010**, *22*, 2228–2246.
12. Rim, Y. S.; Lim, H. S.; Kim, H. J. Low-Temperature Metal-Oxide Thin-Film Transistors Formed by Directly Photopatternable and Combustible Solution Synthesis. *ACS Appl. Mater. Interfaces* **2013**, *5*, 3565–3571.
13. Lim, H. S.; Rim, Y. S.; Kim, H. J. Photoresist-Free Fully Self-Patterned Transparent Amorphous Oxide Thin-Film Transistors Obtained by Sol−Gel Process. *Sci. Rep.* **2014**, 4.

14. Hennek, J. W.; Kim, M.-G.; Kanatzidis, M. G.; Facchetti, A.; Marks, T. J. Exploratory Combustion Synthesis: Amorphous Indium Yttrium Oxide for Thin-Film Transistors. *J. Am. Chem. Soc.* **2012**, *134*, 9593–9596.
15. Kim, G. H.; Shin, H. S.; Du Ahn, B.; Kim, K. H.; Park, W. J.; Kim, H. J. Formation Mechanism of Solution-Processed Nanocrystalline Ingazno Thin Film as Active Channel Layer in Thin-Film Transistor. *J. Electrochem. Soc.* **2009**, *156*, H7–H9.
16. Jeong, S.; Ha, Y. G.; Moon, J.; Facchetti, A.; Marks, T. J. Role of Gallium Doping in Dramatically Lowering Amorphous-Oxide Processing Temperatures for Solution-Derived Indium Zinc Oxide Thin-Film Transistors. *Adv. Mater.* **2010**, *22*, 1346–1350.
17. Calzada, M.; González, A.; Poyato, R.; Pardo, L. Photosensitive Sol−Gel Solutions for the Low-Temperature UV-Assisted Processing of $PbTiO_3$ Based Ferroelectric Thin Films. *J. Mater. Chem.* **2003**, *13*, 1451–1457.
18. Larkin, P. *Infrared and Raman Spectroscopy: Principles and Spectral Interpretation*; Elsevier: Amsterdam, 2011.
19. Yoon, M.-C.; Choi, Y. S.; Kim, S. K. The OH Production from the $\pi-\pi^*$ Transition of Acetylacetone. *Chem. Phys. Lett.* **1999**, *300*, 207–212.
20. Nagashima, N.; Kudoh, S.; Takayanagi, M.; Nakata, M. UV-Induced Photoisomerization of Acetylacetone and Identification of Less-Stable Isomers by Low-Temperature Matrix-Isolation Infrared Spectroscopy and Density Functional Theory Calculation. *J. Phys. Chem. A* **2001**, *105*, 10832–10838.
21. Zhang, X.; Yang, J.; Zeng, Z.; Wu, Y.; Huang, L.; Chen, Y.; Wang, H. Photopolymerization and Initiating Mechanism of Michael Addition Oligomers without Photoinitiator. *Polym. Eng. Sci.* **2007**, *47*, 1082–1090.
22. Mahadevan, E. G. *Ammonium Nitrate Explosives for Civil Applications: Slurries, Emulsions and Ammonium Nitrate Fuel Oils*; Wiley-VCH: Weinheim, Germany, 2013; pp 15−30.
23. Cho, H.; Douglas, E. A.; Scheurmann, A.; Gila, B. P.; Craciun, V.; Lambers, E. S.; Pearton, S. J.; Ren, F. Al_2O_3/$InGaZnO_4$ Heterojunction Band Offsets by X-ray Photoelectron Spectroscopy. *Electrochem. Solid-State Lett.* **2011**, *14*, H431–H433.